

Evidence of under-developed torus and broad-line region of weak emission line quasars based on their spectral energy distribution

Ritish Kumar^{1*}, Hum Chand¹, Ravi Joshi²

¹ *Department of Physics and Astronomical Science, Central University of Himachal Pradesh.*

² *Indian Institute of Astrophysics, Koramangla, Bangalore, 560034, India*

Accepted —. Received —; in original form —

ABSTRACT

To unravel the dominant cause of the weak emission line in a subset of optically selected radio-quiet ‘weak emission line quasars’ (WLQs), we have investigated the possibility of an underdeveloped broad line region (BLR). For this, we have modeled spectral energy distributions (SED) of 61 WLQs by using their optical and infrared (IR) photometric observations from SDSS and WISE respectively. SED fit consists of various emission components, including the luminosity from the dusty torus (L_{tor}). For comparison with the normal quasar, we have used a control sample of 55 QSOs for each WLQs matching in emission redshift and SDSS r-band. Based on our measurement of L_{tor} , we found a decrement of $42 \pm 2\%$ in IR-luminosity in WLQs w.r.t the control sample of normal QSOs. Using L_{tor}/L_{bol} as the measure of torus covering factor (CF_{tor}) we found a similar decrement in WLQs covering factor, with their CF_{tor} distribution being significantly different w.r.t. the normal QSOs with a KS-test P_{null} of 4.27×10^{-14} . As dusty torus and BLR covering factors are expected to be of a similar order in AGN, our results suggest that the BLR in the WLQs is underdeveloped and could be a dominant cause of the weakness of their emission line. As a result, our analysis gives support to the models of WLQs based on the evolution scenario being in an early stage of AGNs.

Key words: galaxies: active – Galaxies: galaxies: jets – Galaxies : (galaxies:) quasars : general – Galaxies: (galaxies:) BL Lacertae objects: general – Galaxies

1 INTRODUCTION

The key ingredients of a unified model of the AGN central engine are composed of a supermassive black hole in the center along with the various substructures including the accretion disk, broad line region (BLR), and dusty torus. The dusty torus plays a crucial role in absorbing radiation from the central part and re-emitting it in IR, as well as explaining the distinct characteristics of Type-1 and Type-2 AGN based on their different orientation relative to the line of sight (Antonucci 1993; Urry & Padovani 1995). The BLR region has high-velocity gas ($\text{FWHM} = 1000\text{--}20,000 \text{ km s}^{-1}$) being embedded in the gravitational potential well of a quasar’s supermassive black hole (SMBH). The high energy photons (UV and/or X-ray) from the accretion disk and corona photo-ionize the gas in BLR, giving rise to prominent broad emission lines with a rest-frame equivalent width (EW_r) of about 50–110 Å for typical Ly α +N v emission line in quasars (e.g., see Schneider et al. 1991; Francis et al. 1993; Osmer et al. 1994; Warren et al. 1994; Zheng et al. 1997; Brotherton et al. 2001; Dietrich et al. 2002). However, these lines can either disappear or appear much weaker (typically, $\text{EW}_r < 15 \text{ Å}$ for

Ly α + N v) for a subclass of BL Lac objects (BLOs) in which optical/UV emission is dominated by the doppler boosted non-thermal continuum from the relativistic jet (e.g., see Begelman et al. 1984). As BLOs are jet dominated (e.g., see Urry & Padovani 1995), they are radio loud having radio to optical flux density ratio, $R^1 > 10$. However, with the advent of large spectroscopic surveys, such as the Sloan Digital Sky Survey (SDSS; e.g., York et al. 2000) and the Two-Degree Field QSO Redshift Survey (2QZ; Boyle et al. 2000), a peculiar or new class of hundreds of high-redshift (mostly at $z > 2$) radio-quiet quasars (RQs) displaying exceptionally weak or even, in some cases completely missing, emission lines were discovered (e.g., see Collinge et al. 2005; Fan et al. 2006; Anderson et al. 2007; Plotkin et al. 2010a,b; Wu et al. 2011; Meusinger & Balafkan 2014). These objects are commonly known as weak emission line quasars (WLQs), various models have been proposed for the observed weak emission lines, including (i) radiatively inefficient accretion flow (RIAF) lead-

¹ Radio loudness (R) is usually parameterized by the ratio of flux densities at 5 GHz and at 2500 Å in the rest frame, being $R > 10$ and $R < 10$ for radio-loud and radio-quiet respectively (e.g., see Kellermann et al. 1989).

* E-mail: ritishshield@gmail.com

ing to intrinsically weaker optical/UV continuum radiation (Yuan & Narayan 2004), (ii) soft ionising continuum causing the weakness of emission lines in BLR (Leighly et al. 2007a,b; Laor & Davis 2011; Wu et al. 2011; Luo et al. 2015), and (iii) anemic or unusual BLR (Shemmer et al. 2010; Nikolaĳuk & Walter 2012), by postulating WLQs being in the early evolutionary phase of quasars (e.g., see Hryniewicz et al. 2010; Liu & Zhang 2011).

On the observation side, many programs have also been carried out to either confirm or refute many of the models mentioned above. For instance, the observed high luminosity of WLQs (e.g., see Meusinger & Balafkan 2014) excludes the possibility of radiatively inefficient accretion flow as the leading cause behind the origin of their weak emission lines. For models based on soft ionizing photons, the possible mechanisms are (i) a cold accretion disk around a supermassive black hole with $M_{BH} > 3.6 \times 10^9 M_\odot$ for non-rotating and $> 1.4 \times 10^{10} M_\odot$ for maximally rotating black hole (Laor & Davis 2011), though based on the measured SMBH mass of WLQs, it also appears to be an unlikely scenario (e.g., see Meusinger & Balafkan 2014; Plotkin et al. 2015), (ii) extremely high accretion rate inducing a soft ionizing continuum (Leighly et al. 2007a,b), however, the observed low fraction of WLQs with such a required high accretion rate also excludes this possibility (e.g., see Nikolaĳuk & Walter 2012). Another possibility is based on the high Eddington ratio in a geometrically thick accretion disk which creates a shielding gas that prevents the BLR from getting photo-ionized by a central continuum source (e.g., see Wu et al. 2011; Luo et al. 2015; Ni et al. 2018; Paul et al. 2022). Sources with weak emission lines may also be obscured AGNs (Ulvestad & Antonucci 1988), where spectropolarimetry is found useful to confirm or refute such possibility of obscuration of the continuum/BLR emission from the direct view (e.g., see Goodrich & Miller 1988).

Alternatively, the BL-Lac nature of WLQs is also tested by comparing the intranight optical variability duty cycle (e.g., see Gopal-Krishna et al. 2013; Chand et al. 2014; Kumar et al. 2015; Kumar et al. 2016, 2017) and nature of their optical polarization (e.g., see Smith et al. 2007; Diamond-Stanic et al. 2009; Heidt & Nilsson 2011; Kumar et al. 2018). Unlike the blazars with higher INOV duty cycle ($\sim 30 - 50\%$) (e.g., see Gopal-Krishna & Wiita 2018) and higher polarization value, the WLQs are found to have a INOV duty cycle of $\sim 5\%$ and polarization of $< 3\%$, thus are more like a normal radio-quiet quasars. These observational pieces of evidence seems to favour the scenario where WLQs might belong to the early phase of AGNs' lifetime rather than being the radio-quiet counterparts of BL Lac. In this evolutionary scenario, the radiation from the spherical cocoon of gas can easily escape through the axis of angular momentum and hence help in the formation of doughnut-shape structure, finally leading to the dusty torus (e.g., see Liu & Zhang 2011, their figure 5). Accordingly, the accretion disk in WLQs will be relatively recently established, and hence the BLR is unlikely to be significantly developed yet (e.g., see Hryniewicz et al. 2010; Liu & Zhang 2011; Andika et al. 2020). This will have its consequences on the covering factor of the BLR in WLQs, to be at least an order of magnitude smaller compared to the normal QSOs, as found in the study of Nikolaĳuk & Walter (2012) based on the ratios of high-ionization line and low-ionization line regions. Additionally, Gaskell et al.

(2007); Gaskell (2009) has argued that the covering factor of BLR and dusty torus has to be the same. This is due to the fact that lower covering factor of torus will lead to BLR in absorption which is not supported by observation (e.g., see Antonucci et al. 1989; Koratkar et al. 1992). Similarly, the torus with a covering factor higher than BLR will be unable to exist due to direct radiation from the central source on its portion not shielded by the BLR (e.g., see Gaskell 2009). For instance, Netzer & Laor (1993) proposed that the outer boundary of the BLR is set by dust formation which is also confirmed by IR reverberation mapping (e.g., see Suganuma et al. 2006; Gaskell et al. 2007), predicting that the covering factor of BLR and dusty torus should be similar. Therefore, in the case of WLQs, if they have an underdeveloped BLR, then the smaller covering factor of the dusty torus will have additional observational consequences in the infrared (IR) band, viz., the reduction of its IR emissivity in comparison to the normal QSOs. To test this hypothesis, a comparison of the infrared spectral energy distribution (SED) of WLQs and normal QSOs matched in their optical luminosity and redshift will be very useful. In this context, Diamond-Stanic et al. (2009) has reported a reduction of about 30–40% in the IR luminosity of two WLQs (viz., SDSS J140850.91+020522.7 with $EW(C\ IV) = 1.95\ \text{\AA}$ and SDSS J144231.72+011055.2 with $EW(C\ IV) = 16.9\ \text{\AA}$). Similarly, Zhang & Liu (2016) have also compared the IR luminosity of normal QSOs with WLQs by using SED fitting, and they have found that WLQs and normal QSOs are statistically similar, though their results are consistent with the evolution scenario. Also, their model of SED fitting was very simplistic, consisting of only the best-fit model of power law and a single-temperature black body. In such a simplistic model, any difference in the IR-luminosity originating from the dusty torus might get diluted in the absence of a proper decomposition of the various emission components of AGN nuclei, such as the AGN inner accretion disk, dusty torus, host galaxy, and the cold dust in star-forming regions. Therefore, to confirm or refute the scenario of the less developed BLR as the cause of the weak emission line in WLQs based on the observed IR emission from the dusty torus, it becomes important to carry out the SED fitting of the large sample of the WLQs by properly decomposing the various components of emissions. This forms the main motivation of the present work. Here we used IR observations of WLQs from the Wide-field Infrared Survey Explorer (WISE; Wright et al. 2010) band in conjunction with their SDSS observation in the optical band, to model the SED of each WLQ and compare it with the SED of control sample of normal QSOs matched in redshift and SDSS r-band magnitude.

The paper is organized as follows: Section 2 describes our sample selection of WLQs and control sample of normal QSOs. In Section 3, we present analysis and results based on SED fitting of our sample, followed by a discussion and conclusions in Section 4. In this paper we assume that $H_0 = 70\text{ km s}^{-1}\text{ Mpc}^{-1}$, $\Omega_\lambda = 0.7$, and $\Omega_M = 0.3$.

2 SAMPLE OF WLQS

Our parent sample consists of WLQs selected from two catalogs based on the SDSS Data Release 7 (DR-7 Abazajian et al. 2009) given by Plotkin et al. (2010a, hereafter PL10)

and Meusinger & Balafkan (2014, hereafter MB14). In table 6 of the PL10 catalog, they have given a list of 86 high-confidence WLQs based on featureless optical spectra and radio-quietness (i.e. $R < 10$). In the catalog of MB14, they employed machine learning data mining techniques to the large database of quasars in the SDSS DR7 pipeline (DR-7; Abazajian et al. 2009). This is followed by manual inspection as well as imposing rest-frame equivalent-width thresholds: $\text{EW}(\text{Mg II}) < 11 \text{ \AA}$ and $\text{EW}(\text{C IV}) < 4.8 \text{ \AA}$, leading to a well-defined sample of 46 WLQs. Out of them, 9 were found to be common with the 86 WLQs taken from PL10, leading to the addition of only 37 WLQs from the MB14 sample. All the 86 WLQs in the PL10 are radio-quiet, having a radio-loudness parameter, $R < 10$. However, among the 37 sources considered from the MB14 catalog, 15 sources were excluded due to their radio-loudness parameter $R > 10$. As a result, we are left with 108 WLQs (86 from PL10 and 22 from MB14) as our initial parental sample. We further checked for the availability of the WISE data for our sample of these 108 WLQs in the compilation of Pâris et al. (2018) in the SDSS DR14 quasar catalog and found that the WISE data is available for 98 WLQs. We have also carried out a visual inspection of the SDSS spectrum of these 98 WLQs and noted that 5 sources were genuinely identified as galaxies and hence reduced our sample to 93 sources. As an extra check for the genuine extra-galactic nature of our sources, we also checked the proper motion of our sources based on the proper motion catalog of Monet et al. (2003). For this, a criterion of proper motion to be either zero or consistent with zero at $< 2.5\sigma$ level is adopted (e.g., see Kumar et al. 2015). This criterion excluded 12 sources with significant proper motion and led us to a sample of 81 sources. Further, we have also excluded 4 sources belonging to crowded fields due to the high possibility of contamination of their photometric fluxes (to be used in our SED fit), leading to a sample of 77 sources. For the comparison of the SED of the WLQs with the normal quasars, we have made the control sample of normal quasars matching in redshift and r-band magnitude with WLQs within the tolerance of ≤ 0.01 and ≤ 0.6 mag, respectively. The chosen tolerance limits are found optimal to get 55 normal QSOs control samples for each WLQ except 8 WLQs. These 8 WLQs belong either to very low ($0.04 < z < 0.06$) or very high ($3.5 < z < 6.5$) redshift ranges, resulting in scarcity of sources for the control sample within the tolerance limits. This led to our sample of 69 WLQs sources along with a control sample of 55 normal QSOs for each of them, with details such as name, RA, DEC, optical (u, g, r, i, z) and infrared (W1, W2, W3, W4) magnitude, as given in Table 1 for WLQs as well as in Table 2 for the median properties of the control sample of normal QSOs corresponding to each WLQs.

3 ANALYSIS AND RESULTS

In our analysis of SED fitting, we have used the observed flux value of our WLQs sample and control sample derived from their optical SDSS magnitude in u, g, r, i and z bands, and in IR using the WISE magnitude in W1, W2, W3, and W4 bands as listed in Table 1 and Table 2, respectively. Here in the control sample, we have used the median value of the magnitude of the 55 normal QSOs corresponding to each WLQ and the error bar on the median magnitude is estimated as

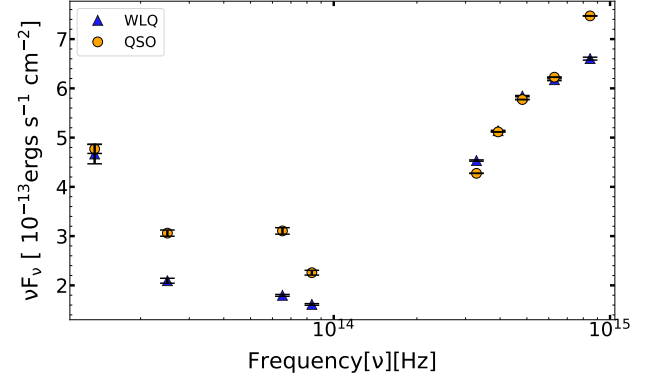


Figure 1. Comparison of median values of the observed flux (νF_ν) of the WLQs sample and the corresponding median value of the control sample of normal quasars. The triangle denotes the WLQs whereas the solid circle denote the normal quasars. The error bars in the median values, obtained by proper error propagation, are smaller than the symbol size.

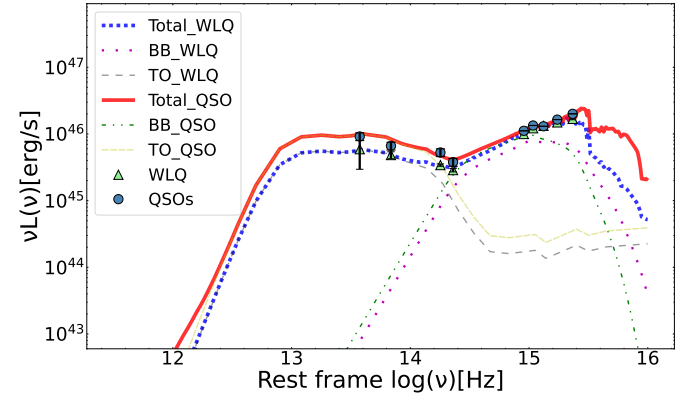


Figure 2. Illustration of the best fit SED comparison of different components of emission in one of the WLQ from our sample, namely J141141.96+140233.9 (solid triangle, thick dotted line) along with SED fit to its corresponding median flux value of the control sample of normal QSOs (solid circle, thick line).

expected on the mean value by propagating the observed error bar of the individual sources. For conversion of SDSS magnitude to flux at the central waveband of the filter, we have used the online platform provided by Gemini² observatory, which is based on SDSS calibrations. For the conversion of WISE magnitude, we have used the formulae

$$F_\nu [Jy] = F_{\nu 0} \times 10^{(-m_{\text{wise}}/2.5)}$$

where $F_{\nu 0}$ is the zero magnitude flux density by assuming the AGN spectrum of the form $F_\nu \propto \nu^{-2}$, as detailed in Wright et al. (2010). In Fig. 1 we show the plot of the median values of the observed flux, at the central frequency of the WISE and SDSS filters, both for 69 WLQs as well as their control sample of normal QSOs. As can be seen from this figure, the

² <https://www.gemini.edu/observing/resources/magnitudes-and-fluxes/conversions-between-magnitudes-and-flux>

Table 1. Basic parameters of the 69 WLQs in our sample.

SN.	Source Name	R.A	Dec	z	$u_{mag} \pm \text{err}$	$g_{mag} \pm \text{err}$	$r_{mag} \pm \text{err}$	$i_{mag} \pm \text{err}$	$z_{mag} \pm \text{err}$	$W_1 \pm \text{err}$	$W_2 \pm \text{err}$	$W_3 \pm \text{err}$	$W_4 \pm \text{err}$
1	J001444.03–000018.5	3.68	−0.005	1.549	18.2 ± 0.02	17.99 ± 0.03	17.87 ± 0.03	17.72 ± 0.02	17.58 ± 0.02	14.98 ± 0.04	13.96 ± 0.04	11.29 ± 0.2	8.34 ± 0.04
2	J001514.88–103043.6	3.81	−10.51	1.170	19.59 ± 0.05	19.57 ± 0.03	19.23 ± 0.02	19.1 ± 0.02	19.03 ± 0.06	15.71 ± 0.05	14.79 ± 0.07	12.07 ± 0.38	8.81 ± 0.05
3	J001741.87–105613.2	4.42	−10.94	1.806	19.22 ± 0.03	19.00 ± 0.03	18.8 ± 0.02	18.64 ± 0.02	18.63 ± 0.04	16.06 ± 0.06	14.73 ± 0.06	11.51 ± 0.21	8.75 ± 0.06

Note: The entire table is available in online version. Only a portion of this table is shown here to display its form and content.

Table 2. Median values of the basic parameters of the control sample corresponding to the 69 WLQs in our sample.

SN.	Source Name*	$u_{mag} \pm \text{err}$	$g_{mag} \pm \text{err}$	$r_{mag} \pm \text{err}$	$i_{mag} \pm \text{err}$	$z_{mag} \pm \text{err}$	$W_1 \pm \text{err}$	$W_2 \pm \text{err}$	$W_3 \pm \text{err}$	$W_4 \pm \text{err}$
1	J001444.03–000018.5	18.40 ± 0.00	18.09 ± 0.00	17.96 ± 0.00	17.74 ± 0.00	17.74 ± 0.00	14.55 ± 0.13	13.15 ± 0.13	10.06 ± 0.13	7.87 ± 0.13
2	J001514.88–103043.6	19.70 ± 0.01	19.55 ± 0.00	19.22 ± 0.00	19.2 ± 0.00	19.27 ± 0.01	15.53 ± 0.13	14.33 ± 0.13	11.48 ± 0.13	8.66 ± 0.13
3	J001741.87–105613.2	19.06 ± 0.00	18.89 ± 0.00	18.80 ± 0.00	18.52 ± 0.00	18.51 ± 0.00	15.48 ± 0.13	14.20 ± 0.13	10.94 ± 0.13	8.43 ± 0.13

Note: The entire table is available in online version. Only a portion of this table is shown here to display its form and content.

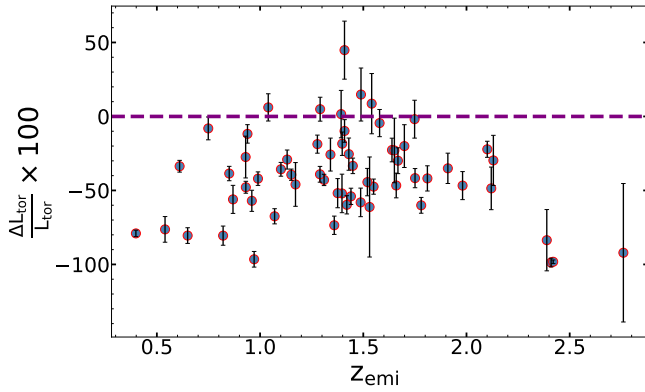


Figure 3. The plot show $\Delta L_{tor}/L_{tor} (\equiv [L_W^{tor} - L_Q^{tor}]/L_Q^{tor})$ verses emission redshift (z_{emi}), computed for each member of the WLQ with respect to its control sample of normal QSOs. It can be noticed that (i) except few outliers, all the WLQs shows smaller torus luminosity in comparison to their redshift and r-band magnitude matched sample of normal QSOs, (ii) there is no significant trend in the $\Delta L_{tor}/L_{tor}$ as a function of emission redshift.

WISE flux, especially in W1, W2, and W3, is systematically smaller for WLQs in comparison to their control sample of normal QSOs. The quantification of this difference (in observed frame) requires proper decomposition of SED (in rest frame) into its individual emission components, as detailed in the next section.

3.1 SED fitting using AGNFITTER

The observed value of the flux at the central wavelength of the WISE and SDSS filters is used to fit the SED of each WLQ and the composite of their control sample, consisting of 55 normal QSOs, by using the publically available code AGNFITTER³ as detailed in Calistro Rivera et al. (2016). In brief, AGNFITTER disentangles the physical processes responsible for AGN emission, such as the contribution from

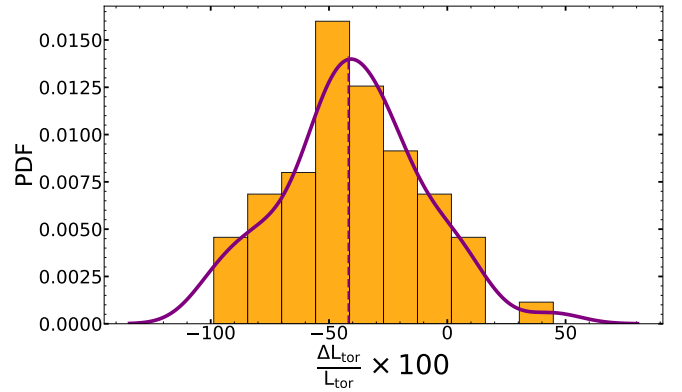


Figure 4. The kernel smooth probability distribution function (PDF) of the percentage deviation of torus luminosity of WLQs with respect to the control sample of QSOs ($\Delta L_{tor}/L_{tor}$). The median percentage deviation $\Delta L_{tor}/L_{tor}$ is found to be $-42 \pm 2\%$. The Gaussian function fit to this distribution results in a typical 1σ uncertainty of 29%.

the stellar populations of the host galaxy, cold dust in star-forming regions, hot dusty torus, and AGN accretion disk. The SED can be constructed using model templates that depict the contribution of each source component at different wavelength ranges, including UV and optical wavelengths to sub-millimeters.

The SED of AGNs contains significant features in the ultraviolet to optical region known as the “Big Blue Bump” (BBB). The BBB is thought to originate from an optically thick accretion disk accreting matter into SMBH, whose energy contribution generally peaks at extreme ultraviolet wavelength regime (e.g., see Mathews & Ferland 1987). Modeling of BBB in AGNFITTER is done by using the modified version of the empirical template given by Richards et al. (2006) which was derived based on composite spectrum obtained by using 259 Type-1 QSOs. The reddening law for this template was given by Prevot et al. (1984), which is found to be effective in treating reddening seen in Type-1 AGNs (e.g., see Hopkins et al. 2004; Salvato et al. 2008). In their modification, they have independently modeled the mid-IR regime by using the warm

³ <https://github.com/GabrielaCR/AGNfitter>

Table 3. The best fit parameters of SED fit based on AGNFITTER for our sample of 61 WLQs.

SN.	Source Name	τ	SB	BB	GA	TO	EBV_{bb}	EBV_{gal}	Age	N H	L_{IR}	L_{bb}	$L_{bbdered}$	L_{ga}	L_{tor}	L_{sb}
1	J001444.03–000018.5	8.75	2.23	2.97	3.88	2.50	0.10	0.05	5.68	21.29	46.63	46.39	46.7	46.2	46.19	45.97
2	J001514.88–103043.6	7.17	1.99	2.31	4.98	2.00	0.05	0.10	9.39	21.37	46.52	45.64	45.8	45.07	45.45	45.84
3	J001741.87–105613.2	6.39	2.24	2.45	3.61	2.39	–0.04	0.27	6.47	21.38	46.27	46.29	46.29	45.37	46.19	45.6

Note: The entire table is available in online version. Only a portion of this table is shown here to display its form and content.

Table 4. The best fit parameters of SED fit based on AGNFITTER for the composite spectrum of control sample corresponding to each of our 61 WLQs.

SN.	Source name*	τ	SB	BB	GA	TO	EBV_{bb}	EBV_{gal}	Age	N H	L_{IR}	L_{bb}	$L_{bbdered}$	L_{ga}	L_{tor}	L_{sb}
1	J001444.03–000018.5	8.02	2.25	2.92	3.97	2.8	0.1	0.1	6.48	21.76	44.01	46.34	46.64	46.13	46.46	43.41
2	J001514.88–103043.6	10.16	1.67	2.28	3.58	2.28	0.05	–0.04	8.13	21.26	43.99	45.61	45.78	45.04	45.72	43.28
3	J001741.87–105613.2	6.94	2.16	2.67	3.32	2.61	0.1	–0.04	5.48	21.3	43.85	46.21	46.52	45.97	46.42	43.22

Note: The entire table is available in online version. Only a portion of this table is shown here to display its form and content.

Table 5. The median value of the important parameters of our SED model fit based on 61 WLQs and using their corresponding composite of their control sample of normal QSOs.

Parameter*	WLQ	σ_{wlq}	QSO	σ_{qso}	%deviation $\left[\frac{WLQ-QSO}{QSO} \times 100 \right]$
SB	1.99 ± 0.22	1.68	1.84 ± 0.23	1.78	5.93 ± 19.17
BB	2.49 ± 0.01	0.11	2.62 ± 0.001	0.003	-2.15 ± 0.52
GA	4.29 ± 0.05	0.39	3.52 ± 0.004	0.03	23.01 ± 1.44
TO	2.35 ± 0.03	0.24	2.57 ± 0.01	0.05	-8.59 ± 1.20
EBV _{bb}	0.06 ± 0.01	0.08	0.10 ± 0.01	0.02	-6.27 ± 15.47
EBV _{gal}	0.20 ± 0.01	0.09	-0.034 ± 0.004	0.03	-138.38 ± 130.06
L _{dered} (0.1–1 μm)	14.09 ± 0.42	3.32	19.12 ± 0.02	0.15	-11.81 ± 1.81
L _{ga} (0.1–1 μm)	5.16 ± 0.15	1.17	6.28 ± 0.01	0.06	-5.75 ± 7.37
L _{tor} (1–30 μm)	8.85 ± 0.51	4.002	13.99 ± 0.29	2.32	-41.69 ± 1.59

*SB, BB, GA, TO refers to normalization parameters of “starburst”, “big blue bump”, “galaxy” and “torus” component respectively.

*EBV_{bb}, EBV_{gal} refers to the reddening parameters of “big blue bump” and “galaxy” component respectively.

*L_{dered}, L_{ga}, L_{tor} refers to the luminosity of “deredened big blue bump”, “galaxy” and “torus” component respectively. in unit of 10^{45} erg/s.

dust template (e.g. Calistro Rivera et al. 2016). The dusty torus components in AGNFITTER are modeled using the empirical template given by Silva et al. (2004). For estimating the host galaxy contribution, a stellar population synthesis model of Bruzual & Charlot (2003) is used. Cold dust emission from the star-forming regions is modeled by using 169 templates with a wide range of SED shapes and luminosities (e.g., see Chary & Elbaz 2001; Dale & Helou 2002). We have individually fitted the SED for each of the 69 WLQs and their corresponding fit of the median flux of their control sample of normal quasars, using AGNFITTER, by converting the observed flux value to their rest-frame value. Further, to use the ratio of IR-luminosity to the bolometric luminosity (L_{bol}) as a measure of covering factor of duty torus, we used the value L_{bol} from the literature. Out of the total 69 sources, the L_{bol} for 61 sources we have taken from Rakshit et al. (2020), and for 5 sources taken from the NASA/IPAC database⁴ and the remaining 3 sources without proper L_{bol} were excluded from our sample, reducing the sample to 66

sources. Lastly, we noticed in our SED fitted value of torus luminosity for 5 sources does not satisfy the physical condition of $L_{tor} < L_{bol}$, and hence got excluded. This led to the final sample of 61 WLQs sources and the corresponding 61 SED fit of the median flux of the control sample consisting of 55 normal QSOs. The SED fits to our entire sample of 61 WLQs is given in online mode in Fig. A, however, for illustration in Fig. 2, we have shown our SED comparison of different components for one of the WLQs in our sample, namely J141141.96+140233.9, along with the corresponding fit of the median fluxes of its control sample of normal QSOs.

3.2 Dusty torus luminosity and covering factor

AGNFITTER provides a list of various parameters associated with different components. Among them, few important are: (i) contribution from big blue bump (BBB) along with its reddening ($E(B-V)_{bb}$), (ii) torus emission parameterised by torus luminosity ($L_{tor}(1-30\mu m)$), torus column density, (iii) stellar emission parameterised by star formation time scale ($\tau[Myr]$), Galaxy age, reddening ($E(B-V)_{gal}$)

⁴ <https://ned.ipac.caltech.edu/>

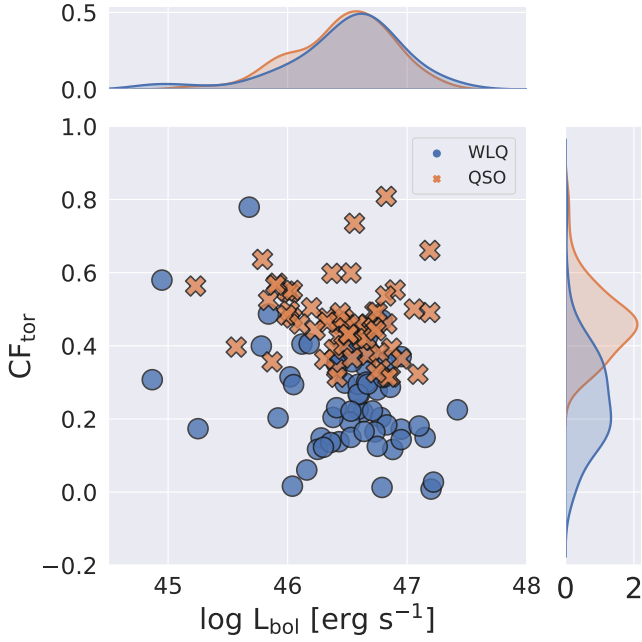


Figure 5. Correlation between the covering factor of the torus (CF_{tor}) and the bolometric luminosity L_{bol} . The blue dot represents the WLQs whereas the orange cross represents the control sample of QSOs.

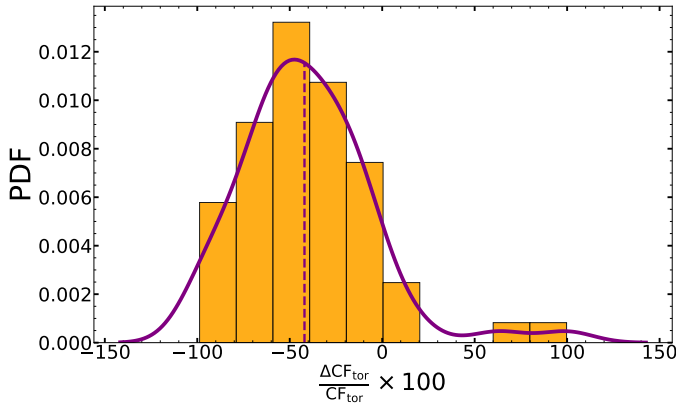


Figure 6. The kernel smooth probability distribution function (PDF) of the percentage deviation of torus covering factor of WLQ with respect to the QSOs ($\Delta CF_{tor}/CF_{tor}$). The median percentage deviation $\Delta CF_{tor}/CF_{tor}$ is found to be $-42 \pm 4\%$.

and luminosity ($L_{gal}(0.1 - 1\mu m)$). The best-fit parameters of the SED fit of each of the 61 WLQs in our sample and their corresponding fit of the median fluxes of control sample of normal QSOs are given in Table 3 and Table 4, respectively. These parameters in AGNFITTER are extracted based on their various realizations and the corresponding associated errors by using 16th and 84th-percentile realizations relative to the median 50th-percentile value, assuming the distribution function to be Gaussian. The scatter plot of $\Delta L_{tor}/L_{tor} (\equiv [L_{tor}^{WLQ} - L_{tor}^{QSO}]/L_{tor}^{QSO})$ with emission redshift (z_{emi}) for our sample of 61 WLQs is shown in Fig. 3. As can

be seen from this figure that (i) except for a few outliers, all WLQs shows smaller torus luminosity in comparison to their redshift and r-band magnitude matched sample of normal QSOs and (ii) the $\Delta L_{tor}/L_{tor}$ do not show any visual trend with the z_{emi} with their Pearson correlation coefficient of -0.094 . This non-significant correlation of $\Delta L_{tor}/L_{tor}$ with z_{emi} allows us to carry out the statistical study of the entire sample even though our WLQs sample belongs to a range in z_{emi} (0.5 to 3.0). The median values of these parameters in 61 WLQs, and the percentage deviation of WLQs w.r.t the SED fit of the median flux of its control sample of normal QSOs are given in Table 5. In Fig. 4 we have plotted the kernel smooth probability distribution function (PDF) of $\Delta L_{tor}/L_{tor}$. As can be seen from this figure that $\Delta L_{tor}/L_{tor}$ distribution is clearly showing smaller L_{tor} for WLQs with median value of $\Delta L_{tor}/L_{tor}$ to be $42 \pm 2\%$. The Gaussian function fit to this distribution results in a typical 1σ uncertainty of 29%, and got the bolometric luminosity from there. In total, we have 66 sources among 69 sources for which we have bolometric luminosity. Our estimated L_{tor} can also be used to estimate the covering factor of a torus (CF_{tor}), in conjunction with the available L_{bol} measurements, as $CF_{tor} = L_{tor}/L_{bol}$ (e.g., see Zhang & Liu 2016). The plot of CF_{tor} with L_{bol} along with distributions of CF_{tor} both for WLQs as well as normal QSOs are shown in Fig. 5. As can be seen from this figure, the L_{bol} distribution of WLQs and QSOs are similar with KS-test P_{null} of 0.82, but the distribution of CF_{tor} is significantly different with KS-test P_{null} of 4.27×10^{-14} , being systematically lower for WLQs. Since L_{bol} also includes the contribution from the L_{tor} , to check its impact on the derived result we also estimated the covering factor as $L_{tor}/(L_{bol} - L_{tor})$ and found the percentage decrement of 61% which is higher than the 42% based on the use of L_{tor}/L_{bol} . However, for the sake of comparison with earlier studies, we have adhered to the definition of covering factor of dusty torus as L_{tor}/L_{bol} . In Fig. 6 we plot the kernel smooth probability distribution function of the percentage deviation of torus covering factor, $\Delta CF_{tor}/CF_{tor} (\equiv [CF_{tor}^{WLQ} - CF_{tor}^{QSO}]/CF_{tor}^{QSO})$, which clearly shows the decrement in the covering factor of WLQs with a median value of about $-42 \pm 4\%$.

4 DISCUSSION AND CONCLUSIONS

With the advent of large spectroscopic surveys, various techniques have been used to unravel the nature of the enigmatic population of WLQs, especially in the context of testing two main scenarios: (i) insufficient ionizing photons as the cause of weak emission lines in WLQs and (ii) WLQs being in the early phase of quasar evolution where BLR is yet to be fully developed. As suggested by Gaskell (2009), such under-developed BLR will also suggest the low covering factor of the dusty torus, which will result in the decrement of IR-emission (e.g., see Sec. 1). To test this hypothesis, we have carried out the SED fitting of 61 WLQs and compared them with the control sample of the normal QSOs, matching in redshift and r-band magnitude (e.g., see Sec. 2). With our detailed SED modeling (e.g., see Sec. 3) the median value of $\Delta L_{tor}/L_{tor}$ is found to be -0.42 ± 0.02 with typical r.m.s scatter from the median of about 0.29 (e.g., see Fig. 4), suggesting that the torus luminosity of WLQs is about 42% lower in comparison

to the redshift and (optical) luminosity matched sample of the normal QSOs.

Our results are consistent with many earlier studies suggesting that WLQs are in the AGN stage of the early phase of their evolution, where BLR has not yet fully developed and hence results in weak emission lines. For instance, [Diamond-Stanic et al. \(2009\)](#) reported that two WLQs are fainter in the IR band by 30-40% (e.g., see Sec. 1). On the other hand, [Zhang & Liu \(2016\)](#) have also carried out SED fitting of 73 WLQs, where although they did not find any significant difference in the SED of the WLQs and normal QSOs, their results were also supporting the evolution scenario for WLQs, where due to much larger scale of torus it should form before the formation of BLR. It may be noted that the procedure of SED fitting used in [Zhang & Liu \(2016\)](#), only involved components of power-law and black-body. However, in our SED fitting, we have carefully decomposed the various components of emission, which has allowed us to separate out the emission coming from the dusty torus. For comparison with normal QSOs, our study for the first time makes use of control sample matching in redshift and r-band magnitude. These two improvements have perhaps allowed us to detect the difference in torus luminosity of WLQs and normal QSOs, which was missing in the oversimplified aforementioned model used in [Zhang & Liu \(2016\)](#), in spite of the fact that the majority of sources in our sample overlap with their sample. Moreover, we also stress here that our results presented here are based on the comparison of WLQs SED fit with their redshifted and r-band luminosity matched control sample. As a result, any unknown systematics in observation and/or in SED modeling will not affect our above results of percentage deviation both regarding the torus (IR) luminosity as well as in the torus covering factor.

We also note that the emission redshift of our WLQs sample (hence of the redshift-matched control sample as well) varies over a wide range from 0.5 to 3.0. However, as can be seen from Fig. 3, the relative change of torus luminosity does not show any correlation with redshift. This non-evolution of L_{tor} with redshift enables us to compare statistically the distribution of the entire sample of WLQs with the control sample of normal QSOs, resulting in the aforementioned $42 \pm 2\%$ IR-luminosity decrement in WLQs w.r.t the control sample of normal QSOs, comprising a 3σ range of 36% to 48%. For individual sources also, it can be noted from Fig. 3 that the L_{tor} of WLQs is found to be consistently smaller in comparison to the control sample of normal QSOs, for all the individual sources in our sample except few outliers (being less than 10 percent). The distribution of $\Delta L_{tor}/L_{tor}$ is well fitted with Gaussian with a best fit mean of -0.39 ± 0.04 and σ of 0.29. The large value of σ ($= 0.29$) suggests that individual measurements of $\Delta L_{tor}/L_{tor}$ still have high uncertainty, which needs to be reduced either statistically by enlarging the sample size as employed in our study here or by using a large number of photometric data points in SED fit, such as by adding UV and X-ray data in future as well. It can also be noted that the error on the median (i.e., $\sim 2\%$) obtained after error propagation is almost half of the value obtained on the mean (i.e., $\sim 4\%$) based on the σ of the $\Delta L_{tor}/L_{tor}$ distribution. This could be either due to the error under-estimation in flux (i.e., magnitude) or over-estimation of the r.m.s scatter due to a few outliers. Nevertheless, to be on the conservative side, even if we took the higher conservative uncertainty

(i.e., 4% on median value), the decrement detected here in IR-luminosity in WLQs w.r.t the control sample of normal QSOs still deviates from zero at high significance with 3σ range of -30% to -54% around the measured value of 42%.

Based on the measured width of the emission line, we notice that all the sources in our sample are Type-I AGNs, so it is unlikely that the decrement in IR flux in WLQs can be attributed to any an-isotropic emission of BBB component if it arises from the accretion disk, as such an effect would be dominant in the sample dominated by Type-II AGNs. We also note that the photometric data points used in optical-based on SDSS and in IR-based on WISE are not simultaneous. As a result, our SED fit implicitly assumes that the variation of WLQs and/or of QSOs used in our sample is not very significant. This could be a reasonable assumption as both WLQs and normal QSOs show nominal variation, unlike the highly variable sources such as BL Lacs and blazar (e.g., see [Diamond-Stanic et al. 2009](#); [Shemmer et al. 2010](#); [Nikolajuk & Walter 2012](#); [Kumar et al. 2018](#)). Moreover, our study used a reasonably large sample, so any nominal variation between the epoch of IR and optical photometric observation in any individual source should not have any significant effect on our above statistical result. Further, we also noted that in our r-band magnitude matched sample of WLQ and normal QSOs, the possibility of the emission line flux contribution will be more in QSOs (due to strong emission lines) than in WLQs (due to weak emission lines). This implies that the intrinsic continuum of WLQs (having less contamination of emission lines) may be brighter (in optical and hence in IR as well) than their control sample of normal QSOs (matched in r-band magnitude). As a result, the actual decrement of IR flux in WLQs might be more than 42% as we have found here. The other possibility, in the context of our result of WLQs being in the early phase of AGN evolution, maybe the episodic phase of the AGN. However, observationally, AGN's episodic activities are mainly inferred based on episodic changes in their brightness or recurring jet activities (e.g., see [Saikia & Jamrozy 2010](#); [Khrykin et al. 2016](#)), typically giving an episodic time scale of a few million years. In this scenario, if the WLQs phase is a new emerging episode of AGN activity, then it may be in the phase of growing brightness due to restarted AGN activities without destroying the BLR. This might lead to more decrement in continuum and hence increase the measured equivalent width of the emission line, contrary to the systematically smaller EW in WLQs. It suggests that the WLQs maybe perhaps in the early phase of AGN's formation rather than belonging to any episodic phase.

The lower L_{tor} will also have additional consequences in lowering the torus covering factor (CF_{tor}) estimated as L_{tor}/L_{bol} . As can be seen from Fig. 5 that the distribution CF_{tor} for WLQs is significantly lower than that of the normal QSO, with KS-test P_{null} of 4.27×10^{-14} . This results in a median percentage decrement of $\Delta CF_{tor}/CF_{tor} = 42 \pm 4\%$ (e.g., see Fig. 6) with a typical r.m.s scatter from the median of about 35%, suggesting that the torus covering factor of WLQs on an average is about 42% smaller with a 3σ of -30% to -54% than that of the normal QSOs of similar redshift and optical luminosity. The covering factor of the torus and the BLR has to be of a similar order (e.g., [Antonucci et al. 1989](#); [Netzer & Laor 1993](#); [Suganuma et al. 2006](#); [Gaskell et al. 2007](#); [Gaskell 2009](#)), so from our above results, we conclude that the BLR in the WLQs is underde-

veloped and it can be a dominant cause of the weakness of their emission line. This gives support to the model of WLQs proposed based on their evolution scenario where WLQs are a special stage in the early phase of AGNs.

ACKNOWLEDGMENTS

We thank the referee Professor Robert R. J. Antonucci for his critical comments and helpful suggestions on the manuscripts. RK and HC are grateful to Gabriela Calistro-Rivera for making the code AGNFITTER public, and IUCAA for the hospitality under IUCAA associate programme.

DATA AVAILABILITY

The data used in this study are publicly available in the SDSS DR14 and WISE All-Sky Data Release.

REFERENCES

- Abazajian K. N. et al., 2009, *ApJS*, 182, 543
- Anderson S. F. et al., 2007, *AJ*, 133, 313
- Andika I. T. et al., 2020, *The Astrophysical Journal*, 903, 34
- Antonucci R., 1993, *Annual review of astronomy and astrophysics*, 31, 473
- Antonucci R. R. J., Kinney A. L., Ford H. C., 1989, *ApJ*, 342, 64
- Begelman M. C., Blandford R. D., Rees M. J., 1984, *Reviews of Modern Physics*, 56, 255
- Boyle B. J., Shanks T., Croom S., Smith R., Miller L., Loaring N., Heymans C., 2000, *Monthly Notices of the Royal Astronomical Society*, 317, 1014
- Brotherton M., Tran H. D., Becker R., Gregg M. D., Laurent-Muehleisen S., White R., 2001, *The Astrophysical Journal*, 546, 775
- Bruzual G., Charlot S., 2003, *Monthly Notices of the Royal Astronomical Society*, 344, 1000
- Calistro Rivera G., Lusso E., Hennawi J. F., Hogg D. W., 2016, *Astrophysical journal*, 833, 98
- Chand H., Kumar P., Gopal-Krishna, 2014, *MNRAS*, 441, 726
- Chary R., Elbaz D., 2001, *The Astrophysical Journal*, 556, 562
- Collinge M. J. et al., 2005, *AJ*, 129, 2542
- Dale D. A., Helou G., 2002, *The Astrophysical Journal*, 576, 159
- Diamond-Stanic A. M. et al., 2009, *ApJ*, 699, 782
- Dietrich M., Hamann F., Shields J., Constantin A., Vestergaard M., Chaffee F., Foltz C., Junkkarinen V., 2002, *The Astrophysical Journal*, 581, 912
- Fan X. et al., 2006, *AJ*, 131, 1203
- Francis P., Hooper E. J., Impey C. D., et al., 1993, *AJ*
- Gaskell C. M., 2009, *New Astronomy Reviews*, 53, 140
- Gaskell C. M., Klimek E. S., Nazarova L. S., 2007, *arXiv preprint arXiv:0711.1025*
- Goodrich R. W., Miller J. S., 1988, *ApJ*, 331, 332
- Gopal-Krishna, Joshi R., Chand H., 2013, *MNRAS*, 430, 1302
- Gopal-Krishna, Wiita P. J., 2018, *Bulletin de la Societe Royale des Sciences de Liege*, 87, 281
- Heidt J., Nilsson K., 2011, *A&A*, 529, A162
- Hopkins P. F. et al., 2004, *The Astronomical Journal*, 128, 1112
- Hryniewicz K., Czerny B., Nikolaïjuk M., Kuraszewicz J., 2010, *MNRAS*, 404, 2028
- Kellermann K. I., Sramek R., Schmidt M., Shaffer D. B., Green R., 1989, *AJ*, 98, 1195
- Khrykin I., Hennawi J., McQuinn M., Worseck G., 2016, *The Astrophysical Journal*, 824, 133
- Koratkar A. P., Kinney A. L., Bohlin R. C., 1992, *ApJ*, 400, 435
- Kumar P., Chand H., Srianand R., Stalin C. S., Petitjean P., Gopal-Krishna, 2018, *MNRAS*, 479, 5075
- Kumar P., Gopal-Krishna, Chand H., 2015, *MNRAS*, 448, 1463
- Kumar P., Hum C., Gopal-Krishna, 2016, *Monthly Notices of the Royal Astronomical Society*, 461, 666
- Kumar P., Stalin C., Chand H., Srianand R., Petitjean P., 2017, *Monthly Notices of the Royal Astronomical Society*, 471, 606
- Laor A., Davis S. W., 2011, *MNRAS*, 417, 681
- Leighly K. M., Halpern J. P., Jenkins E. B., Casebeer D., 2007a, *ApJS*, 173, 1
- Leighly K. M., Halpern J. P., Jenkins E. B., Grupe D., Choi J., Prescott K. B., 2007b, *ApJ*, 663, 103
- Liu Y., Zhang S. N., 2011, *ApJ*, 728, L44
- Luo B. et al., 2015, *The Astrophysical Journal*, 805, 122
- Mathews W. G., Ferland G. J., 1987, *ApJ*, 323, 456
- Meusinger H., Balafkan N., 2014, *A&A*, 568, A114
- Monet D. G. et al., 2003, *AJ*, 125, 984
- Netzer H., Laor A., 1993, *ApJ*, 404, L51
- Ni Q. et al., 2018, *Monthly Notices of the Royal Astronomical Society*, 480, 5184
- Nikolaïjuk M., Walter R., 2012, *MNRAS*, 420, 2518
- Osmer P. S., Porter A. C., Green R. F., 1994, *The Astrophysical Journal*, 436, 678
- Pâris I. et al., 2018, *Astronomy & Astrophysics*, 613, A51
- Paul J. D. et al., 2022, *The Astrophysical Journal*, 929, 78
- Plotkin R. M. et al., 2010a, *AJ*, 139, 390
- Plotkin R. M., Anderson S. F., Brandt W. N., Diamond-Stanic A. M., Fan X., MacLeod C. L., Schneider D. P., Shemmer O., 2010b, *ApJ*, 721, 562
- Plotkin R. M. et al., 2015, *ApJ*, 805, 123
- Prevot M., Lequeux J., Maurice E., Prévot L., Rocca-Volmerange B., 1984, *Astronomy and Astrophysics*, 132, 389
- Rakshit S., Stalin C., Kotilainen J., 2020, *The Astrophysical Journal Supplement Series*, 249, 17
- Richards G. T. et al., 2006, *The Astrophysical Journal Supplement Series*, 166, 470
- Saikia D., Jamrozy M., 2010, *arXiv preprint arXiv:1002.1841*
- Salvato M. et al., 2008, *The Astrophysical Journal*, 690, 1250
- Schneider D. P., Schmidt M., Gunn J. E., 1991, *AJ*, 101, 2004
- Shemmer O. et al., 2010, *The Astrophysical Journal Letters*, 722, L152
- Silva L., Maiolino R., Granato G. L., 2004, *Monthly Notices of the Royal Astronomical Society*, 355, 973
- Smith P. S., Williams G. G., Schmidt G. D., Diamond-Stanic A. M., Means D. L., 2007, *ApJ*, 663, 118
- Suganuma M. et al., 2006, *ApJ*, 639, 46
- Ulvestad J. S., Antonucci R. R. J., 1988, *ApJ*, 328, 569
- Urry C. M., Padovani P., 1995, *PASP*, 107, 803
- Warren S. J., Hewett P. C., Osmer P. S., 1994, *The Astrophysical Journal*, 421, 412
- Wright E. L. et al., 2010, *The Astronomical Journal*, 140, 1868
- Wu J. et al., 2011, *ApJ*, 736, 28
- York D. G. et al., 2000, *AJ*, 120, 1579
- Yuan F., Narayan R., 2004, *The Astrophysical Journal*, 612, 724
- Zhang X., Liu Y., 2016, *The Astrophysical Journal*, 830, 69
- Zheng W., Kriss G. A., Telfer R. C., Grimes J. P., Davidsen A. F., 1997, *The Astrophysical Journal*, 475, 469